doi:10.1016/j.jmb.2009.07.038 *J. Mol. Biol.* (2009) **392**, 803–812

JMB

Available online at www.sciencedirect.com

ScienceDirect

ELSEVIER

Dynamics and Stability in Maturation of a T=4 Virus

Jinghua Tang[1,2], Kelly K. Lee[1], Brian Bothner[1], Timothy S. Baker[2], Mark Yeager[3] and John E. Johnson[1]*

[1]*Department of Molecular Biology, The Scripps Research Institute, La Jolla, CA 92037, USA*

[2]*Department of Chemistry and Biochemistry, and Division of Biological Sciences, University of California, San Diego, La Jolla, CA 92093-0378, USA*

[3]*Department of Cell Biology, The Scripps Research Institute, La Jolla, CA 92037, USA*

Received 2 April 2009; received in revised form 11 July 2009; accepted 14 July 2009
Available online 20 July 2009

Nudaurelia capensis ω virus is a T=4, icosahedral virus with a bipartite, positive-sense RNA genome. Expression of the coat protein gene in a baculovirus system was previously shown to result in the formation of procapsids when purified at pH 7.6. Procapsids are round, porous particles (480 Å diameter) and have T=4 quasi-symmetry. Reduction of pH from 7.6 to 5.0 resulted in virus-like particles ($VLP_{5.0}$) that are morphologically identical with authentic virions, with an icosahedral-shaped capsid and a maximum dimension of 410 Å. $VLP_{5.0}$ undergoes a maturation cleavage between residues N570 and F571, creating the covalently independent γ peptide (residues 571–641) that remains associated with the particle. This cleavage also occurs in authentic virions, and in each case, it renders the morphological change irreversible (i.e., capsids do not expand when the pH is raised back to 7.6). However, a non-cleavable mutant, N570T, undergoes the transition reversibly ($NT_{7.6} \leftrightarrow NT_{5.0}$). We used electron cryo-microscopy and three-dimensional image reconstruction to study the icosahedral structures of $NT_{7.6}$, $NT_{5.0}$, and $VLP_{5.0}$ at about 8, 6, and 6 Å resolution, respectively. We employed the 2. 8-Å X-ray model of the mature virus, determined at pH 7.0 ($XR_{7.0}$), to establish (1) how and why procapsid and capsid structures differ, (2) why lowering pH drives the transition, and (3) why the non-cleaving $NT_{5.0}$ is reversible. We show that procapsid assembly minimizes the differences in quaternary interactions in the particle. The two classes of 2-fold contacts in the T=4 surface lattice are virtually identical, both mediated by similarly positioned but dynamic γ peptides. Furthermore, quasi and icosahedral 3-fold interactions are indistinguishable. Maturation results from neutralizing the repulsive negative charge at subunit interfaces with significant differentiation of quaternary interactions (one 2-fold becomes flat, mediated by a γ peptide, while the other is bent with the γ peptide disordered) and dramatic stabilization of the particle. The γ peptide at the flat contact remains dynamic when cleavage cannot occur ($NT_{5.0}$) but becomes totally immobilized by noncovalent interactions after cleavage ($VLP_{5.0}$).

Keywords: virus structure; virus assembly; virus maturation; cryoEM; maturation cleavage

Edited by W. Baumeister

**Corresponding author.* E-mail address: jackj@scripps.edu.

Present addresses: K. K. Lee, Department of Medicinal Chemistry, University of Washington, Seattle, WA 98195-7610, USA; B. Bothner, Department of Chemistry and Biochemistry, Montana State University, Bozeman, MT 59717, USA; M. Yeager, Department of Molecular Physiology and Biological Physics, University of Virginia Health System, Charlottesville, VA 22908-0736, USA.

Abbreviations used: NωV, *Nudaurelia capensis* ω virus; CP, coat protein; VLP, virus-like particle; IG, immunoglobulin; cryoEM, electron cryo-microscopy; 3D, three-dimensional.

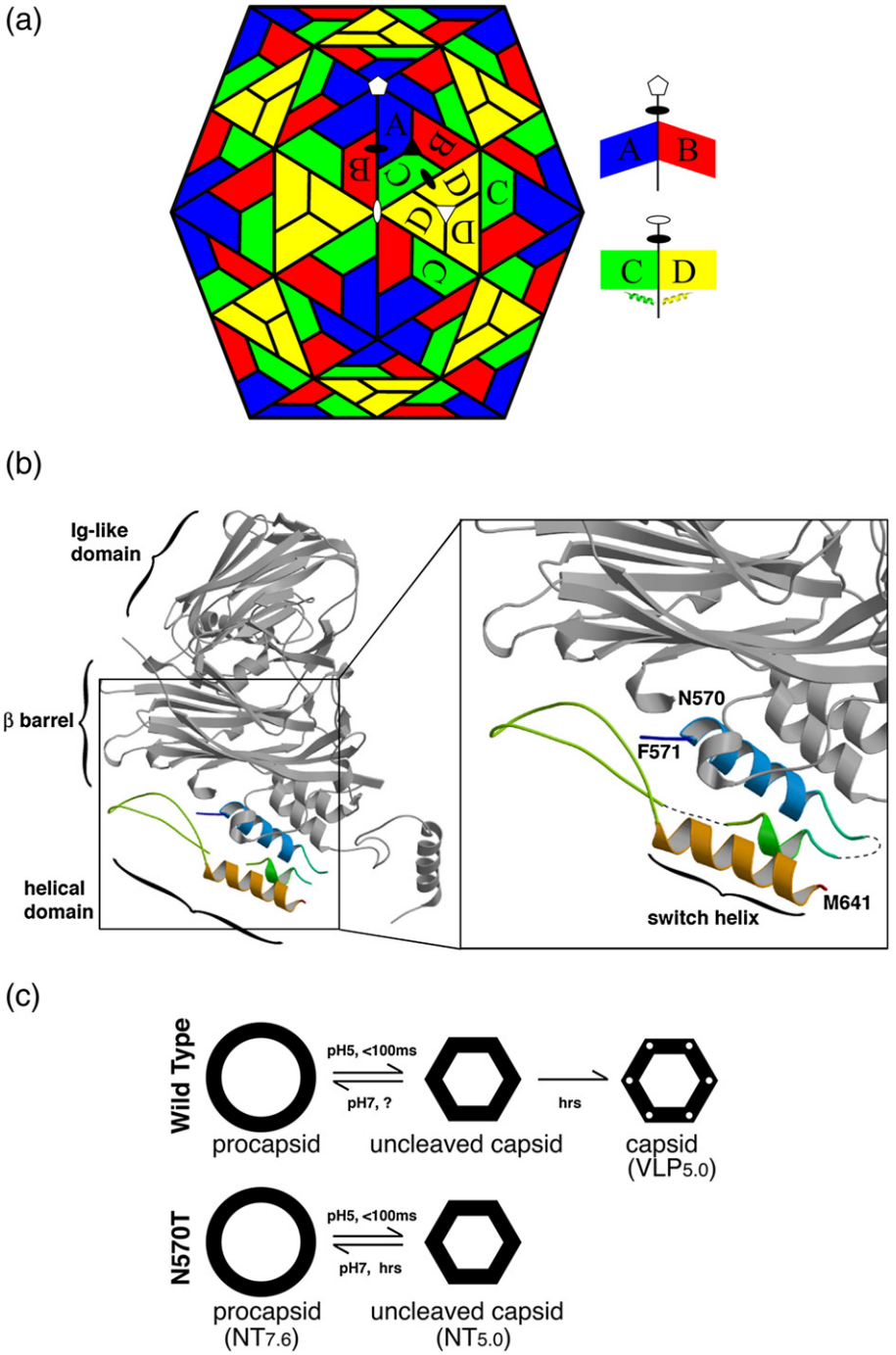

Fig. 1. (a) Schematic diagram of the subunit organization in the T=4 NωV capsid. The four subunits in each asymmetric unit are A (blue), B (red), C (green), and D (yellow). White symbols identify icosahedral symmetry axes, and black symbols identify quasi-2-fold (ellipses) and quasi-3-fold (triangle) axes. Dimer interfaces at the quasi-2-folds occur with bent (A–B) or flat (C–D) conformations. Well-ordered C-terminal helices in the C and D subunits stabilize the flat C–D interface. (b) Ribbon diagram of the C subunit tertiary structure showing the three-domain organization present in all subunits. Maturation cleavage occurs in the inner helical domain between residues Asn570 and Phe571. The γ peptide (colored blue to red from its N- to C-termini) includes a three-helix, two-loop motif. The molecular switch (switch helix) only occurs in the C and D subunits. (c) Procapsid–capsid transitions in wild type and mutant particles. In WT virus, a drop in pH rapidly converts procapsids to uncleaved capsids, followed by slower maturation cleavage, which locks the particle in the capsid conformation. In the cleavage-defective mutant N570T (NT), particle transitions are reversible.

Introduction

Particle maturation is an integral part of the assembly of complex viruses.[1] Initiation of assembly occurs when virally encoded protein subunits interact tenuously with one another, and possibly with nucleic acid, to produce unstable procapsid particles. Procapsid assembly is achieved through a process of self-correcting, intersubunit annealing that places capsid proteins into quasi-equivalent positions in an icosahedral surface lattice. Given an external cue (often a change in pH), this procapsid is programmed by the subunit tertiary and particle quaternary structures to undergo reorganization into a more stable particle ("capsid") that may also undergo auto-catalytic processes that render particles infectious. Here, we investigate particle maturation in an RNA animal virus to address three questions: (1) How and why do procapsid and capsid structures differ? (2) What drives the transition between these states? (3) Why can capsids that have not undergone a maturation cleavage reversibly revert to the procapsid state, whereas cleaved capsids cannot?

The subject of this study was the *Nudaurelia capensis* ω virus (NωV: family *Tetraviridae*), a nonenveloped virus with a bipartite, positive-sense RNA genome.[2] RNA1 and RNA2 encode the RNA-dependent RNA polymerase and the coat protein (CP) subunit, respectively. The capsid contains 240 chemically identical copies of CP arranged in a T=4 icosahedral lattice (Fig. 1). Expression of the CP gene in a recombinant baculovirus system results in the spontaneous assembly of virus-like particles (VLPs) that package predominantly heterogeneous cellular RNA.[3] VLPs purified from baculovirus at pH 7.6 were found to be round, porous particles of diameter 480 Å. The subunits reorganize into smaller, 410-Å-diameter particles when the pH is lowered to 5.0.[4] This pH-induced transition from procapsid to capsid in VLPs occurs in less than 100 ms based on stop-flow experiments.[5] This process is initially reversible, until an auto-proteolytic cleavage ($t_{1/2} = \sim 30$ min) occurs in at least 15% of the subunits and the virus is then locked in the mature capsid conformation.[5] Analogy with other nonenveloped icosahedral viruses such as poliovirus[6] and flock house virus[7] suggests that autolytic cleavage in NωV is essential for cell entry and its infectivity. *In vivo*, NωV is presumably first assembled as procapsid in the neutral pH condition inside the cell. Then, acidification caused by apoptosis would trigger its maturation and release.[8] With the added stability imparted by maturation, the capsid can then survive the harsh extracellular environment before the next infection. The maturation-dependent cleavage occurs between residues Asn570 and Phe571 and converts the 70-kDa CP precursor (α) into 62-kDa (β) and 8-kDa (γ) peptides, both of which remain associated with the mature capsid.[9] When Asn570 was replaced by Thr to produce the N570T mutant ("NT"), the maturation cleavage was blocked and purified particles could be transformed reversibly between large- and small-particle forms with changes in pH (Fig. 1).[10]

The VLP capsid has the same morphology as the capsid seen in crystals of authentic, infectious virions.[11] The crystal structure of NωV revealed that each 641-amino-acid CP subunit is composed of three domains (Fig. 1). These include an internal helical domain; a central, canonical viral jelly-roll;[12] and an outer, immunoglobulin (Ig)-like domain that is likely involved in interactions with host cell receptors. The asymmetric unit of the icosahedral T=4 capsid consists of four subunits, labeled A (blue), B (red), C (green), and D (yellow) (Fig. 1a). They adopt slightly different tertiary conformations because they occupy quasi-equivalent, quaternary structure environments. The virion crystal structure shows that the C and D γ peptides (amino acids 571–641) each contains an ordered helix (amino acids 626–640), and these switch helices serve as wedges that open the C–D dimer contact and create a flat interface with a dihedral angle of 180° (Fig. 1a). These helices are absent in the A and B subunits because the C-termini of the γ peptides in these subunits are disordered, which allows the A–B interface to adopt a bent conformation with a dihedral angle of 138° (Fig. 1a). Hence, the presence or absence of helices in the γ peptides provides the molecular switch that distinguishes the dimers.

Here, we report on electron cryo-microscopy (cryoEM) and three-dimensional (3D) icosahedral image reconstruction analyses of the NT procapsid at pH 7.6 ($NT_{7.6}$) and the NT capsid at pH 5.0 ($NT_{5.0}$), both of which cannot undergo maturation cleavage, and a VLP at pH 5.0 ($VLP_{5.0}$) that mimics the wild-type, mature capsid and undergoes normal maturation and cleavage. Each of these structures was compared to and interpreted with the X-ray coordinates of the mature, infectious virion crystallized at pH 7.0 ($XR_{7.0}$).[11] Each of these particles is described in Table 1. Together, these data explain the basis for the pH-dependent change in the size of the particle and why the pH 5-induced contraction

Table 1. Nomenclature and structural parameters for particles compared in this study

Sample	Notation	pH	Method	*d* (Å)	*D* (Å)	Morphology	Cleavage	AB	CD	Switch helices
N570T mutant	$NT_{7.0}$	7.6	CryoEM	~8.0	480	Procapsid	No	Flat	Flat	Dynamic
N570T mutant	$NT_{5.0}$	5.0	CryoEM	~6.0	410	Capsid	No	Bent	Flat	Dynamic
VLP	$VLP_{5.0}$	5.0	CryoEM	~6.0	410	Capsid	Yes	Bent	Flat	Fixed
NωV virion	$XR_{7.0}$	7.0	X-ray	2.8	410	Capsid	Yes	Bent	Flat	Fixed

d, approximate resolution; *D*, diameter; AB, dimer interface between subunits A and B; CD, dimer interface between subunits C and D.

of the uncleaved particle (NT) is reversible when the pH is raised to 7 whereas the $VLP_{5.0}$ particle contraction is not reversible. We find that the cleavage in $VLP_{5.0}$ allows the γ peptide to achieve many more noncovalent interactions than occur in the uncleaved $NT_{5.0}$ and that these stabilize the compact form, preventing the reversible expansion after cleavage. Indeed, comparing the ordered density in the cleaved form of the γ peptide with the corresponding regions in the uncleaved form revealed that roughly 20% more of these residues were ordered in the cleaved form than in the uncleaved form. This explanation is different from that previously proposed by Taylor *et al.*, which was based on lower-resolution structures of the procapsid and capsid.[10]

Results

NT procapsid structure at pH 7.6

Structural flexibility and instability of the NωV procapsid have likely contributed to failures at obtaining crystals suitable for X-ray crystallography. We therefore employed cryo-EM 3D reconstruction methods to examine the structure of the NT procapsid at pH 7.6 ($NT_{7.6}$). As peptide cleavage only

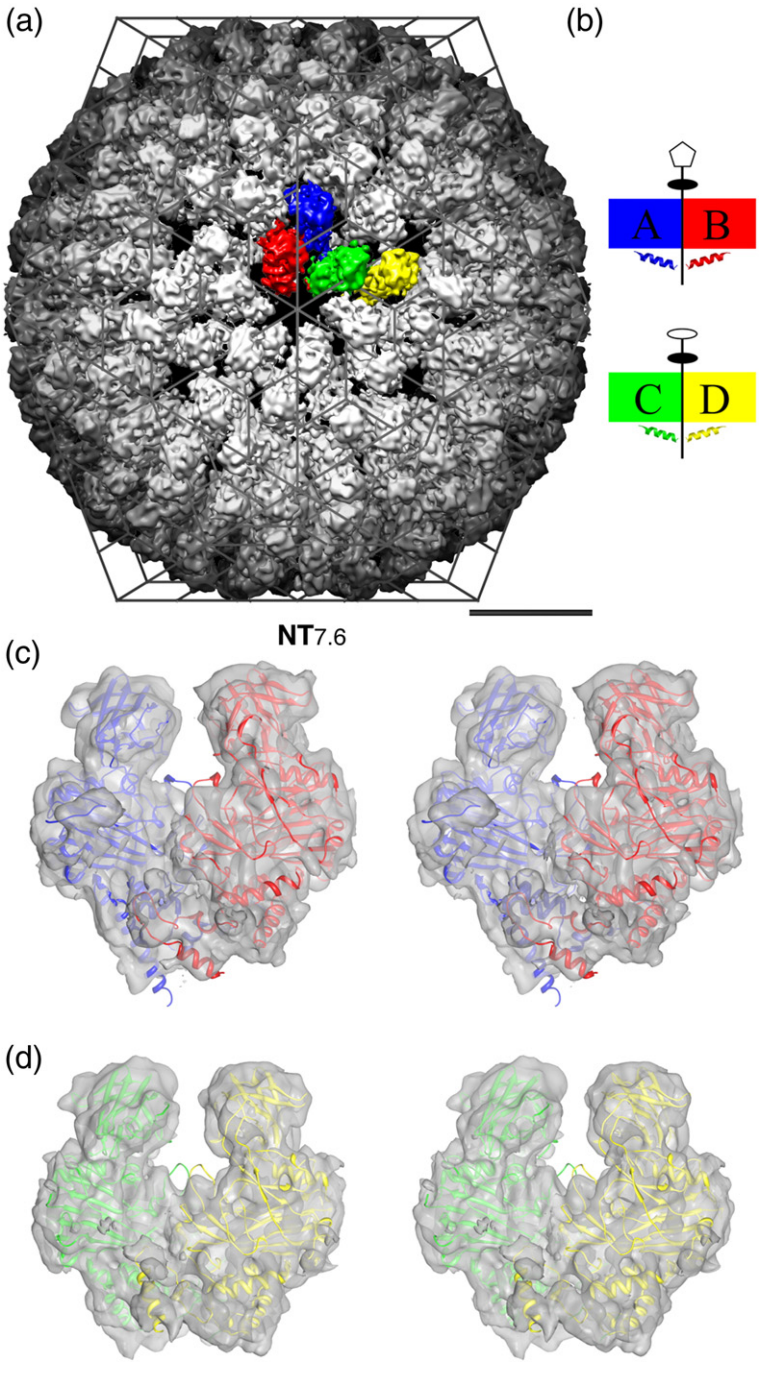

Fig. 2. Eight-angstrom cryoEM reconstruction of the NT procapsid at pH 7.6. (a) Global view of the procapsid outer surface (color coded as in Fig. 1a). (b) Schematic representations of the quasi-2-fold A–B and C–D dimers. (c) Stereo view of the reconstructed density (gray isosurface) for the A–B dimer with an atomic model of each subunit derived from the capsid crystal structure fitted independently into the corresponding density. (d) Same as (c) for the C–D dimer. Similarity of the procapsid A–B and C–D dimer interfaces is apparent because the Ig-like domains maintain a 13-Å separation in both dimers.

occurs in the mature capsid conformation, we anticipated that WT and NT procapsids would have the same structure, and this was indeed verified in cryo-reconstructions performed at 20 Å resolution (data not shown).

The 8-Å cryo-reconstruction of $NT_{7.6}$ shows that the procapsid has a porous surface dominated by openings at the quasi-6-fold (icosahedral 2-fold) axes and closely similar A–B (blue–red) and C–D (green–yellow) subunit dimer contacts (Fig. 2). In each dimer, the Ig domains are separated by 13 Å. The otherwise tenuous particle is held together by close ABC and DDD trimer contacts formed among the inner helical domains. Basic residues dominate the N-terminal portion of the subunits (residues 11–40) that are not visible in the X-ray structure. These residues must contribute to the particle stability (and probably assembly) by interacting with the packaged, heterologous RNA. We constructed a pseudo-atomic model of the procapsid by fitting the coordinates of each capsid subunit from the crystal structure of NωV ($XR_{7.0}$) into the cryoEM density map for one icosahedral asymmetric unit and then refined the four subunits as independent rigid bodies. The dominant-negative surface charge on the subunit interfaces must create significant electrostatic repulsion at pH 7.6 that is balanced by the nucleoprotein interactions to create the procapsid.

Differences in shape and size between procapsid and capsid are primarily attributable to variations in the A–B and C–D dimer interfaces. In capsids, the A–B and C–D interfaces are distinct and exhibit bent (A–B) and flat (C–D) contacts. In the NT procapsid, both interfaces are closely similar to the flat A–B contacts in the capsid (Fig. 2c and d). The procapsid dimers were modeled starting with the C–D dimer from the capsid. The well-ordered switch helices in the capsid are dynamic in the procapsid but, on average, must occupy both of the structurally equivalent dimer interfaces as shown in the pseudo-atomic model (Fig. 3).

Mature (cleaved) capsids at pH 5 and 7 have the same structure

The X-ray structure of the authentic, mature virus ($XR_{7.0}$) was determined with crystals grown at pH 7.0.[11] We compared VLPs at pH 5 with $XR_{7.0}$ coordinates to determine if any portion of the structure changed (particularly within the internal helical region) when fully mature particles were returned to pH 7, the condition where procapsids exist if they have not been exposed to acidic pH. Compact $VLP_{5.0}$ capsids were obtained by incubating procapsids at pH 5.0 for a period of days. This transformation to a more compact structure activates the maturation cleavage that ultimately leads to the virus particle being locked in the capsid conformation (Fig. 1c). The 6-Å $VLP_{5.0}$ cryo-reconstruction closely matched the $XR_{7.0}$ atomic structure (Fig. 4). All of the density in the $VLP_{5.0}$ structure is well accounted for by the X-ray model and indicates that the capsid structure remains essentially unchanged between pH 5 and 7 following maturation. The VLP reconstruction clearly exhibits a break in the density at the cleavage site, consistent with the X-ray model where Asn570 and Phe571 are separated by 8 Å. Thus, within the limits at which such features can be discerned in a reconstruction at 6 Å resolution, there are no detectable differences between the X-ray model and the cryoEM density map. This suggests that conformational reversibility in uncleaved particles is not linked to pH-induced conformational changes in

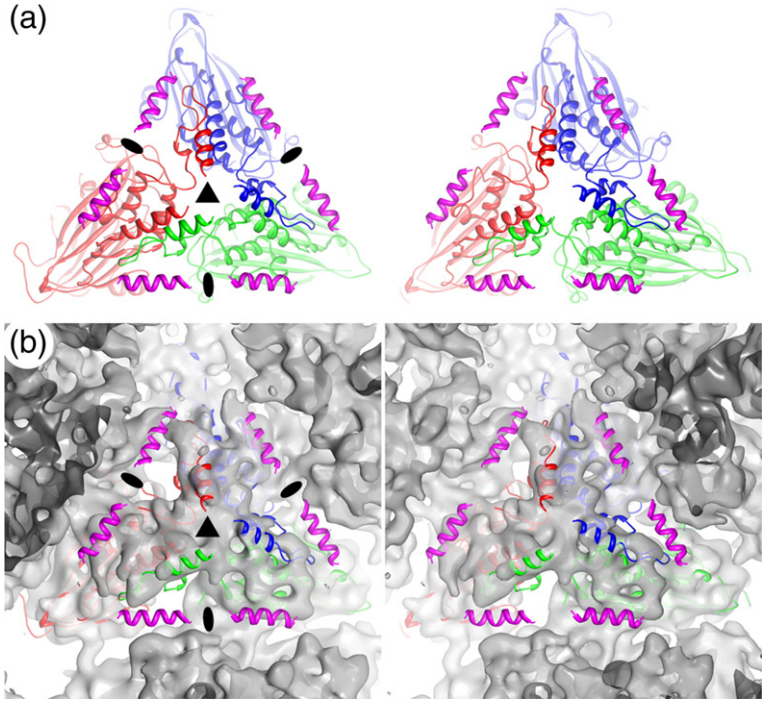

Fig. 3. Pseudo-atomic model of the inner surface of $NT_{7.6}$ centered on the quasi-3-fold trefoil. (a) Stereo ribbon diagram of the modeled, inner helical domains. Filled ellipses identify A–B dimer quasi-2-folds (at left and right) and the C–D dimer quasi-2-fold (at bottom). The trefoil of helices was generated with helix interactions of the A and B subunits observed in $XR_{7.0}$. While those same interactions do not occur in A–C and C–B in $XR_{7.0}$, this 3-fold enforced model fits the trefoil density exceptionally well as shown in (b). The switch helices at the AB and CD interfaces are also shown in the model (purple), although density for these is either completely absent or very weak owing to their dynamic character. (b) Same as (a) with the pseudo-atomic model fit into the $NT_{7.6}$ density map.

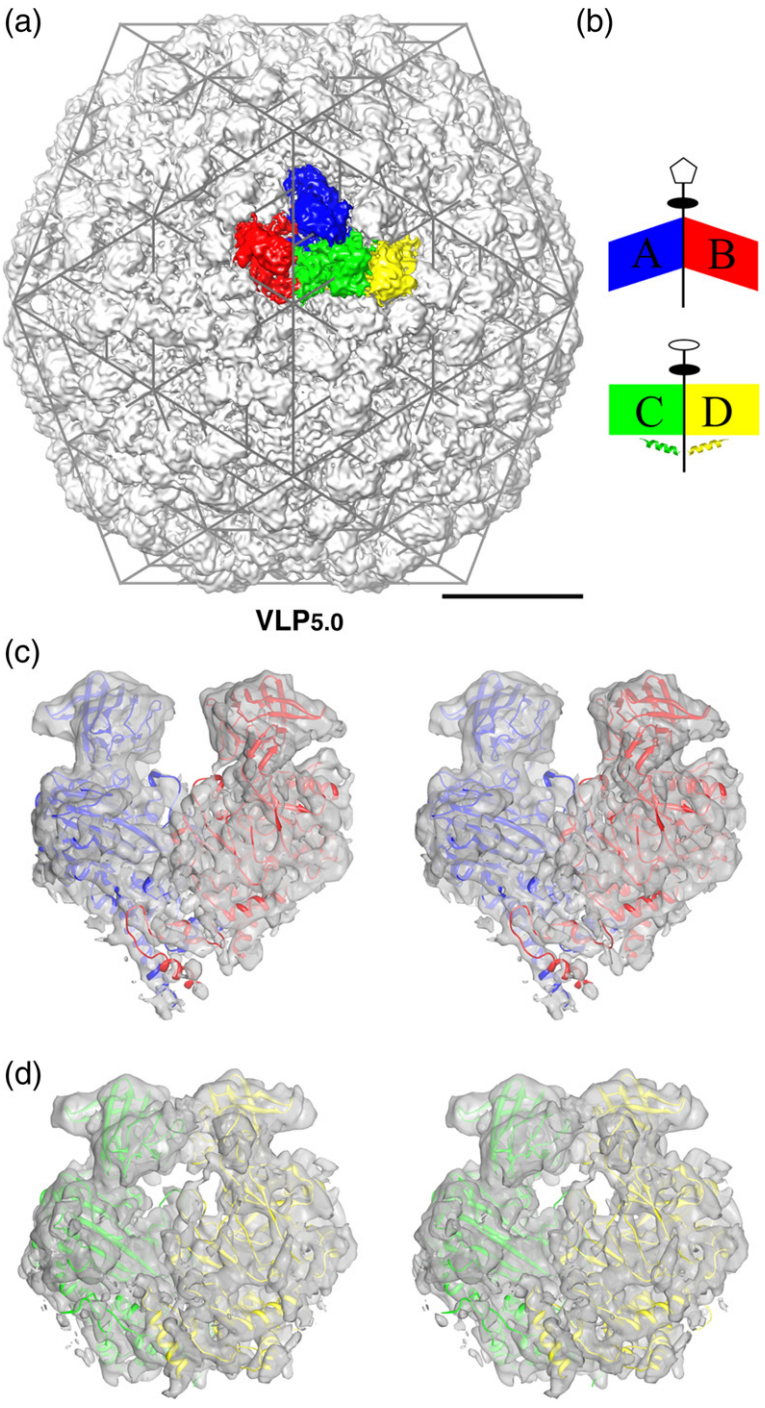

Fig. 4. Six-angstrom cryoEM reconstruction of $VLP_{5.0}$. (a) Global view of the $VLP_{5.0}$ structure (color coded as in Fig. 1a). (b) Schematic representations of the quasi-2-fold A–B and C–D dimers. (c) Stereo view of the reconstructed density (gray isosurface) for the A–B dimer with an atomic model of each subunit derived from the capsid crystal structure fitted independently into the corresponding density. (d) Same as (c) for the C–D dimer. Unlike the procapsid where the Ig-like domains are 13 Å apart in both dimers (Fig. 2), in capsids, the Ig-like domains in the C–D dimer are only 5 Å apart.

the γ peptide as was previously hypothesized (see Discussion).

Structures of cleaved (VLP) and uncleaved (NT) capsids at pH 5 differ

A cryo-reconstruction of the NT (uncleaved) capsid at pH 5 ($NT_{5.0}$) was computed at an estimated resolution of 6 Å. As anticipated, the $NT_{5.0}$ structure showed continuous density at the site where cleavage occurs in wild-type virions and where the density is interrupted in $VLP_{5.0}$ capsids. The density for $NT_{5.0}$ and $VLP_{5.0}$ correlates well in the external, Ig-like domain and also in the middle, jelly-roll domain. However, there are significant differences in the bottom helical domain on the inner surface of the capsid. $NT_{5.0}$ has essentially no density for the switch helices (Fig. 5a), which is in stark contrast to the well-ordered density seen in $VLP_{5.0}$ (Fig. 5b), and implies that there is high mobility or lack of defined structure for this region in $NT_{5.0}$. On average, the region just below the C–D interface must be occupied by protein in NT because hinging is inhibited and the dimer contact is flat. However, the polypeptide in NT is not rigidly fixed as it is in $VLP_{5.0}$.

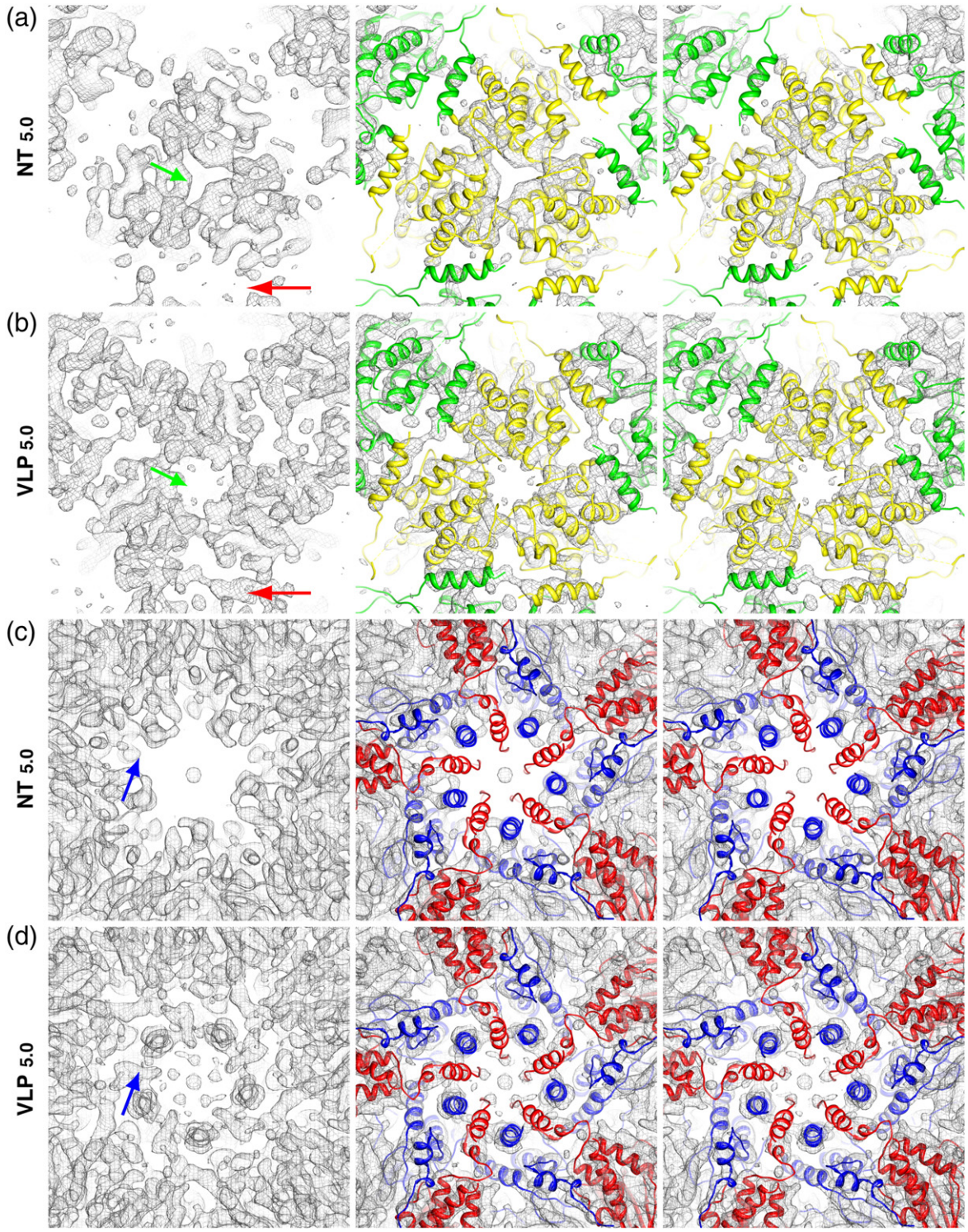

Fig. 5. Comparison of 6-Å electron density for uncleaved ($NT_{5.0}$) and cleaved ($VLP_{5.0}$) capsids at pH 5.0. The first column shows the cryoEM map; the second and third columns are stereo view of the same map superimposed with the $XR_{7.0}$ model. (a and b) Comparison of density for $NT_{5.0}$ and $VLP_{5.0}$ around the 3-fold axis. The green arrows point out that there is more density in the middle of the trimer in $NT_{5.0}$ compared with the $VLP_{5.0}$ structure. Red arrows highlight the switch helices' densities, which are missing at the flat contact in $NT_{5.0}$ and strong $VLP_{5.0}$. This is consistent with reduced dynamic character of the switch helices after maturation cleavage. (c and d) Comparison of the 10-helix bundle at the 5-fold axes in $NT_{5.0}$ and $VLP_{5.0}$. There is no density for residues 44–55 from the B subunit in $NT_{5.0}$, and density for the last eight residues of the A helix (592–599) is missing. In contrast, in $VLP_{5.0}$, the $XR_{7.0}$ model fits the density extremely well, which illustrates that cleavage dramatically reduces the mobility of these helices.

Another region where $NT_{5.0}$ and $VLP_{5.0}$ differ is at the pentamer interface (Fig. 5c and d). $VLP_{5.0}$ density agrees well with the $XR_{7.0}$ coordinates in this region. Here, γ peptide residues 571–599 of the A subunit form a well-ordered helix that interacts with the first helix in the B subunit (amino acids 44–55) to form a 10-helix bundle about each pentamer axis. In contrast, $NT_{5.0}$ shows density only for residues 571–590, and no density is seen for residues 44–55 of the first B subunit helix. Thus, $NT_{5.0}$ has five isolated helices that do not interact with each other, significantly reducing the buried surface area due to the missing helix contribution from the B subunits. Cleavage in $VLP_{5.0}$ particles apparently permits conformational flexibility in the γ peptides and leads to a substantial increase in intersubunit interactions, generating greater stability of mature particles relative to $NT_{5.0}$ (Fig. 6). Thus, at neutral pH, electrostatic repulsions outweigh the modest stability that exists in $NT_{5.0}$, allowing procapsids to reform. This transition is not possible in the cleaved, more stable $VLP_{5.0}$ capsid.

Discussion

The striking feature of the procapsid as observed in the $NT_{7.6}$ reconstruction is the virtual identity of the dyad contacts between A–B and C–D dimers. These contacts occur at low radii, that is, within the capsid shell, whereas those in the external portion of the particle are sparse owing to the presence of the large channels that traverse the capsid at the quasi-6-fold axes. Procapsid stability derives mostly from two sources: protein–nucleic acid interactions contributed by the basic region of the capsid subunit between residues 1 and 40 and the closely similar trimeric contacts in the internal helical domain (corresponding to residues from two neighboring subunits 44–56 and 571–591) in the ABC and DDD trimers. These features are consistent with a mechanism of capsid assembly wherein reversible associations permit chemically identical monomers to organize in a T=4 lattice with minimal difference between quasi-equivalent interactions. The tenuous nature of the procapsid is a consequence of numerous repulsive interactions between charged acidic groups on the surfaces of the subunits. At lower pH, this charge is reduced and this activates the dramatic programmed reorganization of the subunits, leading to closer yet dissimilar contacts within the two classes of dimers. The distinction of these contacts is obvious in the $VLP_{5.0}$ reconstruction and is not detectibly different from what was observed in the crystal structure.[11] Hence, following cleavage, the distinct A–B and C–D interactions persist even when the pH is raised by 2 units. If cleavage is blocked as occurs as in the NT mutant, the entire process of switching between bent and flat A–B contacts is reversible.

A major motivation for this study was to examine our previous hypothesis for the mechanism of reversibility of $NT_{5.0}$. Based on procapsid and capsid cryoEM structures at 20 Å resolution,[4] it was hypo-

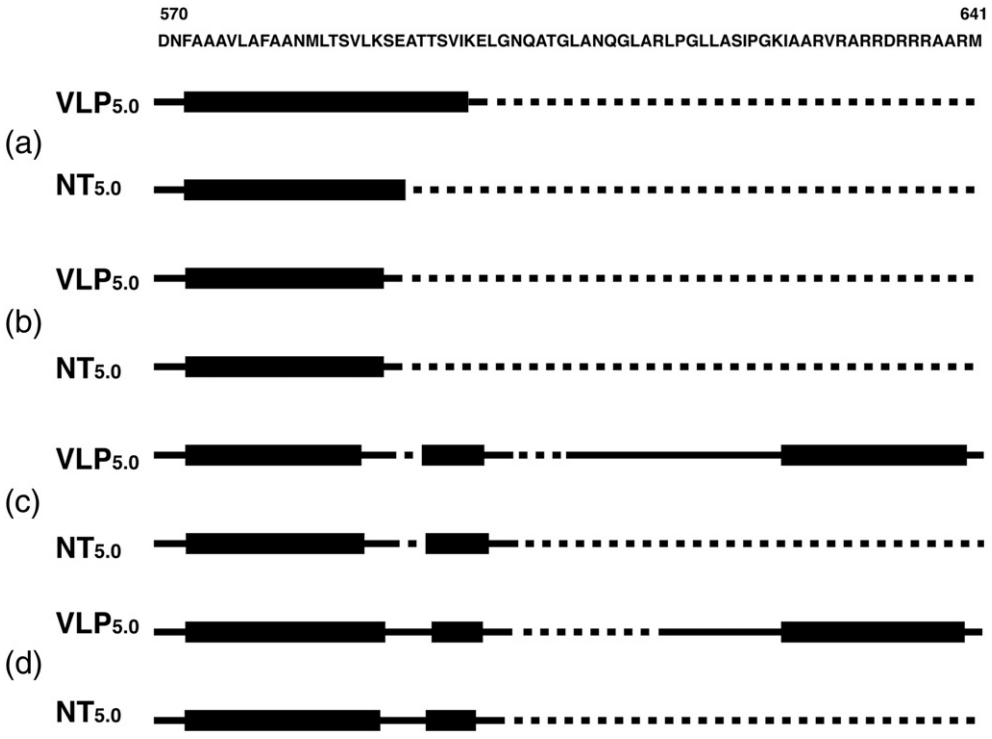

Fig. 6. A diagram comparing portions of the γ peptide that are visible in the electron density for $VLP_{5.0}$ and $NT_{5.0}$. A–D represent the four independent subunits in the icosahedral asymmetric unit of the virus. Ordered and disordered regions were represented by the continuous and dotted lines, respectively. The cleaved $VLP_{5.0}$ contains more ordered regions than the $NT_{5.0}$ structure.

thesized that the γ peptide underwent a pH-dependent helix-to-coil transition and that in turn allowed the procapsid to condense into the more compact capsid.[10] In other words, in the pH 7 (helix) form, the expanded state was maintained, whereas in the pH 5 (coil) form, the subunits could condense. Taylor *et al.* posited that, in the absence of cleavage and hence release of γ peptide, particles would re-expand if the pH were raised back to 7.0 and the region corresponding to the γ peptide reformed the helix. However, with normal cleavage, the pH-dependent structural changes in γ were expected to be uncoupled and pH change would not cause expansion. In contrast to the expectations, the cryoEM data presented here clearly demonstrate that there is no significant difference in the γ peptide regions of $VLP_{5.0}$ and $XR_{7.0}$ and, hence, disprove the previous hypothesis.

The cryo-reconstruction of $NT_{5.0}$ provides the key to understanding the reversible nature of its procapsid-to-capsid transition. In the absence of cleavage, the internal helical domains retain mobility as is evident by numerous regions in $NT_{5.0}$ that have weak or no density when compared to $VLP_{5.0}$ and $XR_{7.0}$. Thus, cleavage in $VLP_{5.0}$ provides the required flexibility in the helical regions to generate increased noncovalent interactions and buried surface area sufficient to withstand the electrostatic repulsion at neutral pH that permits $NT_{5.0}$ capsids to expand into $NT_{7.6}$ procapsids.

Materials and Methods

Preparation and purification of VLPs were carried out as described previously.[13] Procapsids were fraction collected in pH 7.6 buffer (250 mM NaCl and 50 mM Tris–HCl) from a clean band in the sucrose gradient. Procapsid-to-capsid conversion was carried out by overnight dialysis at room temperature against pH 5.0 buffer (250 mM NaCl and 50 mM sodium acetate) to allow the capsid to fully mature.

CryoEM was performed with ~1 mg/ml specimen samples, and images were recorded at 50,000× nominal magnification, under low-dose conditions, and at 200 keV on an FEI CM 200 electron microscope as described previously.[14] Micrographs were digitized in a Zeiss SCAI scanner (ZI imaging) at 7-μm intervals and 2×2 bin-averaged to give an effective pixel size of 2.8 Å at the specimen. Individual particle images were boxed from the micrographs with the RobEM program†, and 3D reconstructions were computed with the program suite AUTO3DEM.[15] 3D reconstructions of the $VLP_{5.0}$, $NT_{5.0}$, and $NT_{7.6}$ particles were computed from 8576, 18,205, and 2582 particles, respectively. The resolution limit of each cryo-reconstruction (6 Å for $VLP_{5.0}$ and $NT_{5.0}$ and 8 Å for $NT_{7.6}$) was estimated on the basis of standard Fourier shell correlation criteria, using a 0.5 threshold.[16]

A pseudo-atomic model of the procapsid was built using the atomic coordinates derived from the crystal structure of the capsid ($XR_{7.0}$) as a starting model. We used a modified version[17] of the program Rsref[18] to dock the X-ray model as a rigid body into the $NT_{7.6}$ cryo-reconstruction and then refine it. Programs O[19] and Chimera[20] were used to visualize and analyze the map and model data.

† http://cryoem.ucsd.edu/programDocs/runRobem.txt

Acknowledgements

We thank Mr. Kevin Chiang for help with boxing particle images from micrographs. We thank Bob Sinkovits for computational assistance in upgrading AUTO3DEM. This work was supported by grants from the National Institutes of Health [RO1 GM54076 (to J.E.J.), R01 GM066087 (to M.Y.), and RO1 GM033050 (to T.S.B.)].

Supplementary Data

Supplementary data associated with this article can be found, in the online version, at doi:10.1016/j.jmb.2009.07.038

References

1. Steven, A. C., Heymann, J. B., Cheng, N., Trus, B. L. & Conway, J. F. (2005). Virus maturation: dynamics and mechanism of a stabilizing structural transition that leads to infectivity. *Curr. Opin. Struct. Biol.* **15**, 227–236.
2. Hanzlik, T. N. & Gordon, K. H. (1997). The Tetraviridae. *Adv. Virus Res.* **48**, 101–168.
3. Agrawal, D. K. & Johnson, J. E. (1995). Assembly of the T=4 *Nudaurelia capensis* omega virus capsid protein, post-translational cleavage, and specific encapsidation of its mRNA in a baculovirus expression system. *Virology*, **207**, 89–97.
4. Canady, M. A., Tihova, M., Hanzlik, T. N., Johnson, J. E. & Yeager, M. (2000). Large conformational changes in the maturation of a simple RNA virus, *Nudaurelia capensis* omega virus (NomegaV). *J. Mol. Biol.* **299**, 573–584.
5. Canady, M. A., Tsuruta, H. & Johnson, J. E. (2001). Analysis of rapid, large-scale protein quaternary structural changes: time-resolved X-ray solution scattering of *Nudaurelia capensis* omega virus (NomegaV) maturation. *J. Mol. Biol.* **311**, 803–814.
6. Ansardi, D. C. & Morrow, C. D. (1995). Amino acid substitutions in the poliovirus maturation cleavage site affect assembly and result in accumulation of provirions. *J. Virol.* **69**, 1540–1547.
7. Schneemann, A., Zhong, W., Gallagher, T. M. & Rueckert, R. R. (1992). Maturation cleavage required for infectivity of a nodavirus. *J. Virol.* **66**, 6728–6734.
8. Tomasicchio, M., Venter, P. A., Gordon, K. H., Hanzlik, T. N. & Dorrington, R. A. (2007). Induction of apoptosis in *Saccharomyces cerevisiae* results in the spontaneous maturation of tetravirus procapsids in vivo. *J. Gen. Virol.* **88**, 1576–1582.
9. Agrawal, D. K. & Johnson, J. E. (1992). Sequence and analysis of the capsid protein of *Nudaurelia capensis* omega virus, an insect virus with T=4 icosahedral symmetry. *Virology*, **190**, 806–814.
10. Taylor, D. J., Krishna, N. K., Canady, M. A., Schneemann, A. & Johnson, J. E. (2002). Large-scale, pH-dependent, quaternary structure changes in an

RNA virus capsid are reversible in the absence of subunit autoproteolysis. *J. Virol.* **76**, 9972–9980.
11. Munshi, S., Liljas, L., Cavarelli, J., Bomu, W., McKinney, B., Reddy, V. & Johnson, J. E. (1996). The 2.8 Å structure of a T=4 animal virus and its implications for membrane translocation of RNA. *J. Mol. Biol.* **261**, 1–10.
12. Rossmann, M. G. & Johnson, J. E. (1989). Icosahedral RNA virus structure. *Annu. Rev. Biochem.* **58**, 533–573.
13. Lee, K. K., Tang, J., Taylor, D., Bothner, B. & Johnson, J. E. (2004). Small compounds targeted to subunit interfaces arrest maturation in a nonenveloped, icosahedral animal virus. *J. Virol.* **78**, 7208–7216.
14. Baker, T. S., Olson, N. H. & Fuller, S. D. (1999). Adding the third dimension to virus life cycles: three-dimensional reconstruction of icosahedral viruses from cryo-electron micrographs. *Microbiol. Mol. Biol. Rev.* **63**, 862–922.
15. Yan, X., Sinkovits, R. S. & Baker, T. S. (2007). AUTO3DEM—an automated and high throughput program for image reconstruction of icosahedral particles. *J. Struct. Biol.* **157**, 73–82.
16. Van Heel, M. & Harauz, G. (1986). Resolution criteria for three dimensional reconstruction. *Optik*, **73**, 119–122.
17. Tang, J., Taylor, D. W. & Taylor, K. A. (2001). The three-dimensional structure of alpha-actinin obtained by cryoelectron microscopy suggests a model for Ca(2+)-dependent actin binding. *J. Mol. Biol.* **310**, 845–858.
18. Chapman, M. S. (1995). Restrained real-space macromolecular atomic refinement using a new resolution-dependent electron density function. *Acta Crystallogr., Sect. A: Found. Crystallogr.* **51**, 69–80.
19. Jones, T. A., Zou, J. Y., Cowan, S. W. & Kjeldgaard, M. (1991). Improved methods for binding protein models in electron density maps and the location of errors in these models. *Acta Crystallogr., Sect. A: Found. Crystallogr.* **47**, 110–119.
20. Pettersen, E. F., Goddard, T. D., Huang, C. C., Couch, G. S., Greenblatt, D. M., Meng, E. C. & Ferrin, T. E. (2004). UCSF Chimera—a visualization system for exploratory research and analysis. *J. Comput. Chem.* **25**, 1605–1612.